

# A Vibrational Sum Frequency Spectroscopic Investigation of the Azimuthal Anisotropy and Rotational Dynamics of Methyl-Terminated Si(111) Surfaces

Sergey Malyk,<sup>a)</sup> Fadel Y. Shalhout,<sup>a)</sup> Leslie E. O'Leary,<sup>b)</sup> Nathan S. Lewis,<sup>b)</sup> and Alexander V. Benderskii<sup>a)</sup>

<sup>a)</sup> Department of Chemistry, University of Southern California, Los Angeles, CA 90089

<sup>b)</sup> Division of Chemistry and Chemical Engineering, Beckman Institute, and Kavli Nanoscience Institute, California Institute of Technology, Pasadena, CA

## Supporting Information

The geometry of SFG laser beams and the surface coordinate system are given in Figure S1.

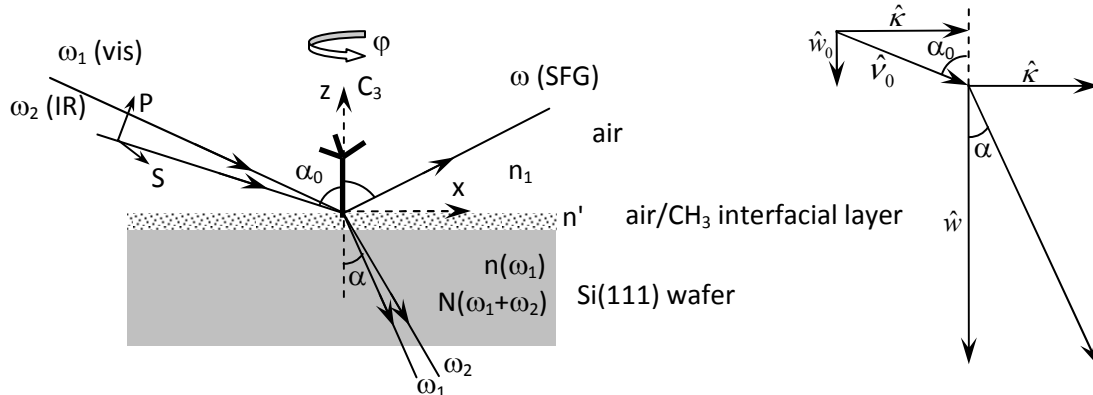


**Figure S1.** Geometry of SFG, surface coordinate system, orientation of the methyl group on Si(111) surface, and the wave vectors and components for the propagating visible field. For the model we assume that  $\alpha$  is approximately the same for  $\omega_1$  and  $\omega_2$ . The refractive index of a Si is  $n$  and  $N$  at  $\omega_1$  and  $(\omega_1+\omega_2)$  respectively.

We have approximated for simplicity that all optical parameters for the IR and visible beams are roughly equal, since both beams incidence angles are roughly the same and the IR and visible beams refractive indices in silicon are very close to each other (3.43 and 3.68 respectively). The component of the visible field wave vector  $\hat{v}_0$  parallel to the surface is given by

$$\kappa = |v_0| \sin(\alpha_0) = \frac{\omega}{c} \sin(\alpha_0). \quad \text{This wave vector is related to the incidence wave vector normal}$$

$w_0$  by  $w_0 = \sqrt{\tilde{\omega}^2 - \kappa^2}$ , where  $\tilde{\omega} = \omega/c$ . We also introduce  $w$  for the medium with dielectric

constant  $\epsilon(\omega_l)$ :  $w = \sqrt{\tilde{\omega}^2 \epsilon(\omega_l) - \kappa^2}$ . The SFG field wave vectors and components can also be

introduced in a similar fashion for the SFG frequency  $\Omega = \omega_l + \omega_2$  by capitalizing the symbols (similar to Sipe et al.<sup>1</sup>). The proportionality constants for bulk isotropic and anisotropic

coefficients can then be written<sup>1</sup>  $A_s = \frac{4\pi \cdot \tilde{\Omega}}{W_0 + W}$ ,  $A_p = \frac{4\pi \cdot \tilde{\Omega} N}{W_0 \cdot \epsilon(\Omega) + W}$ . We additionally introduced

$$D = \frac{n\tilde{\Omega}}{8(2w + W)}. \quad A_p / A_s \sim 1.5 \quad \text{and} \quad D \sim 0.063 \quad \text{for our system was evaluated using above}$$

equations. Below we list the bulk and surface isotropic and anisotropic coefficients given by Sipe et al.<sup>1</sup>:

$$a_{bulk}^s = \frac{4}{3} f_s f_c$$

$$c_{bulk}^s = \frac{4\sqrt{2}}{3} (f_c^2 - f_s^2)$$

$$a_{bulk}^p = \frac{4}{3} F_s f_c - \frac{2}{3} f_s f_c^2 - \frac{8}{3} F_s f_s^2 f_c + \frac{4}{3} f_s^3 F_c$$

$$c_{bulk}^p = F_s f_c^3 - 2 f_s^2 F_c f_c + F_s f_s f_c^2$$

$$a_{surf}^s = 2 \partial_{15} \cdot f_s$$

$$c_{surf}^s = -2\partial_{11} \cdot f_c$$

$$a_{surf}^p = \varepsilon(\omega_1 + \omega_2) \partial_{31} F_s f_c^2 - 2\partial_{15} f_s F_c f_c + \varepsilon(\omega_1 + \omega_2) \partial_{33} F_s f_s^2$$

$$c_{surf}^p = -2\partial_{11} F_c f_c^2$$

where  $F_{s,c}$  are the sine and cosine of the angle of the SFG beam in the silicon,  $f_{s,c}$  are the sine and cosine of the angle of the visible beam in the silicon, and  $\varepsilon(\Omega)$  is the dielectric constant of the medium at the SFG frequency.

A time-delay technique introduced by Lagutchev *et al.*<sup>2</sup> in which the asymmetry of the visible pulse in the time-domain (Fig. S2) is used to up-convert mainly the slower resonant contribution when the IR-visible time delay is judiciously chosen, was used to decouple the nonresonant and resonant signals.

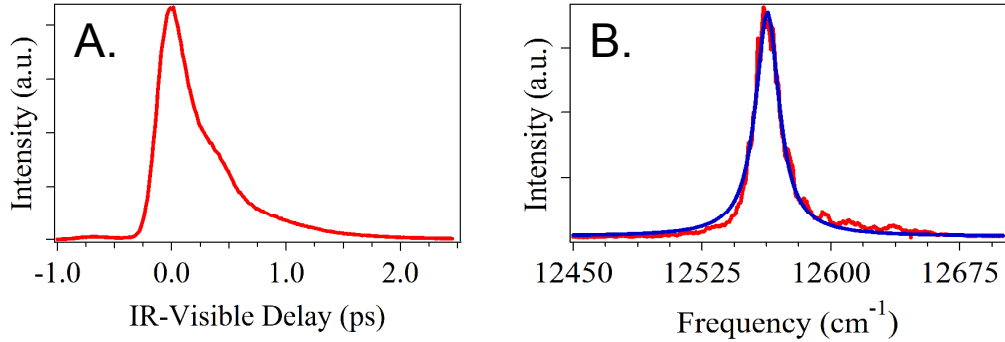


**Figure S2.** (A) Temporal profile of the narrow-band visible pulse. (B) Frequency-domain spectrum (red line) of the narrow-band visible pulse produced by passing the compressed pulse through the etalon. The blue line shows a Lorentzian fit.

As shown in Fig. S3, this technique is particularly advantageous when a considerable nonresonant SFG signal is present, as in the PPP spectra.

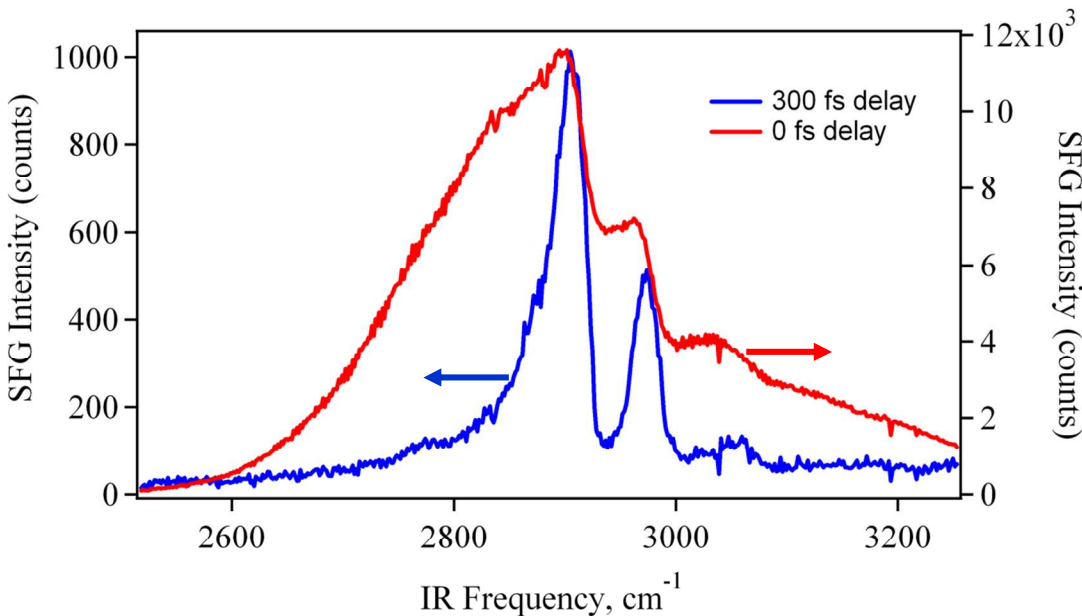


**Figure S3.** Effect of IR-visible time delay on the SFG signal for PPP polarization. Spectra were recorded with zero delay (red line) and 300 fs delay (blue line).

**Table 1.** Fitting parameters for PPP spectra recorded with 0 fs delay between IR and visible pulses.

Rotation angle (deg)	$A_{NR}$ , (a.u.)	$\omega_g$ , (cm $^{-1}$ )	$\sigma_g$ , (cm $^{-1}$ )	$\phi_{NR}$ , (rad)	$B(r^+)$ , (a.u.)	$B(r^-)$ , (a.u.)	$\Gamma(r^+)$ , (cm $^{-1}$ )	$\Gamma(r^-)$ , (cm $^{-1}$ )	$\omega(r^+)$ , (cm $^{-1}$ )	$\omega(r^-)$ , (cm $^{-1}$ )
0	27.0	2870	181	3.3	246	144	14.9	10.8	2917	2977
20	63.0	2897	250	3.2	257	156	14	10	2920	2983
40	65.0	2895	251	3.1	259	156	14	10	2920	2982
60	30.3	2877	197	3.0	264	132	14.4	10	2918	2979
80	33.4	2902	296	-1.5	-436	-276	20	16.5	2915	2975
100	32.7	2903	308	-1.7	-420	-261	20	16.5	2914	2974
120	21.4	2880	182	-2.9	236	155	13.2	11.9	2917	2978
140	63.0	2896	251	3.4	250	139	14	10	2918	2979
160	67.0	2897	251	3.1	262	158	14	10	2919	2982
180	29.0	2878	194	-3.1	274	134	14.4	10	2916	2976
200	34.7	2916	320	-1.5	-430	-240	20	16.5	2913	2971
220	34.9	2923	333	-1.6	-420	-240	20	16.5	2912	2971
240	23.6	2880	173	3.4	251	132	14.4	10	2916	2976
260	63.5	2903	256	3.3	284.2	160	14	10	2917	2979
280	67	2902	252	3.3	270	144	14	10	2916	2980
300	31.4	2875	195	3.2	290	150	14.4	10	2915	2975
320	33.6	2924	323	-1.3	-450	-270	20	16.5	2912	2971
340	34.6	2919	324	-1.5	-446.9	-268	20	16.5	2913	2972

**Table 2.** Fitting parameters for PPP spectra recorded with 300 fs delay between IR and visible pulses.

Rotation Angle, (deg)	$A_{NR}$ , (a.u.)	$\omega_g^+$ , (cm $^{-1}$ )	$\sigma_g^+$ , (cm $^{-1}$ )	$\phi_{NR}$ , (rad)	$B(r^+)$ , (a.u.)	$B(r^-)$ , (a.u.)	$\Gamma(r^+)$ , (cm $^{-1}$ )	$\Gamma(r^-)$ , (cm $^{-1}$ )	$\omega(r^+)$ , (cm $^{-1}$ )	$\omega(r^-)$ , (cm $^{-1}$ )
1.5	9.0	-	-	-2.9	408	-338	12.5	12.0	2915	2975
20	13.7	2991	500	-6.2	605	-398	13.6	10.6	2914	2977
40	14.9	2940	300	-3.1	657	-406	14.2	10.7	2914	2976
60	9.8	-	-	-3.1	473	-315	13.1	12.2	2914	2974
80	17.1	2940	300	0.39	-167	120	14.3	14.0	2907	2979
100	18.4	2920	325	0.3	-133	146	15.0	14.0	2907	2983
120	9.3	-	-	-2.9	431	-363	13.4	12.7	2914	2976
140	16.7	2940	300	-3.3	803	-426	15.5	10.9	2914	2976
160	18.0	2940	300	-3.2	844	-470	16.1	11.2	2914	2975
180	11.4	-	-	-3.2	551	-370	13.5	13.1	2913	2972
200	20.1	2946	351	0.17	-174	140	15.0	14.0	2908	2983
220	23.1	2970	390	0.42	-120	109	16.0	10.0	2907	2975
240	10.7	-	-	-3.2	507	-386	13.4	13.4	2914	2975
260	20.7	2940	300	-2.8	850	-544	17.1	10.6	2913	2975
280	21.8	2940	300	-3.0	973	-544	18.2	10.8	2913	2974
300	12.7	-	-	-3.4	649	-358	14.5	12.4	2914	2973
320	19.8	2940	385	0.42	-180	170	16.0	15.0	2911	2980
340	20.0	2930	410	0.42	-145	175	16.0	13.0	2908	2980
360	10.7	-	-	-3.22	546	-367	14.3	13.0	2915	2976

**Table 3.** Fitting parameters for SSP recorded with 0 fs delay between IR and visible pulses. Amplitudes  $A_{NR}$  and  $B(r^+)$  are normalized with respect to PPP 0 fs delay amplitudes.

$\phi$ , (deg)	$A_{NR}$ , (a.u.)	$\omega_g$ , ( $\text{cm}^{-1}$ )	$\sigma_g$ , ( $\text{cm}^{-1}$ )	$\phi_{NR}$ , (rad)	$B(r^+)$ , (a.u.)	$\Gamma(r^+)$ , ( $\text{cm}^{-1}$ )	$\omega(r^+)$ , ( $\text{cm}^{-1}$ )
0	12.6	2907	234	1.53	109	19.5	2900
20	17.1	2908	282	1.66	84	18.5	2900
40	8.2	2802	188	-0.087	-126	15.3	2907
60	25.3	2845	288	0.32	-231	26	2909
80	25.9	2866	288	0.29	-221	24.8	2910
100	4.9	2875	260	0.29	-55.	16.2	2900
120	13.6	2937	229	1.3	107	19.6	2904
140	15.8	2950	225	1.0	149	22.6	2910
160	6.4	2936	257	-0.01	-104	15.7	2905
180	24.6	2938	330	0.19	-286	33	2912
200	24.0	2926	345	0.24	-255	30.7	2916
205	20.4	2880	332	0.27	-219	27.2	2917
210	6.2	2896	362	0.46	-168	20.3	2913
220	6.7	2924	289	0.25	-160	20.8	2910
230	15.7	2923	192	1.31	186	26.9	2919
240	15.7	2914	244	1.11	186	26.9	2917
250	18.2	2895	292	1.40	133	20.2	2908
260	15.8	2906	288	1.43	136	20	2903
270	10.0	2936	200	1.59	209	34.7	2903
280	6.9	2931	220	-0.17	-126	18.5	2910
290	17.5	2938	229	-0.063	-167	23	2917
300	25.3	2877	326	0.17	-322	35.6	2914
310	29.1	2907	317	0.15	-316	34.8	2914
320	26.9	2908	310	0.107	-319	34	2914
340	6.3	2802	269	0.095	-174	21.8	2905

**Table 4.** Fitting parameters for the rotational anisotropy in resonant and nonresonant amplitudes for PPP and SSP spectra.

	<i>a</i> , (a.u.)	<i>c</i> , (a.u.)	$\phi_0$ , (deg.)	<i>k</i> , (a.u.)
<b>PPP</b>				
$B(r^+)/\Gamma(r^+)$	24.0	36.0	-91	--
$B(r^-)/\Gamma(r^-)$	-20.4	-31.1	-89	--
$A_{NR}$	17.3	50.8	-94	-21
<b>SSP</b>				
$B(r^+)/\Gamma(r^+)$	-3.3	-14.3	159	--
$A_{NR}$	6.9	35.3	153	8.3

**Table 5.** Nonresonant nonlinear susceptibilities of methyl-terminated Si(111) surface obtained by fitting the nonresonant SFG signal for PPP and SSP polarization combinations to equations (14-15)

$\zeta$	$\gamma$	$\partial_{11}$	$\partial_{33}$	$\partial_{31}$	$\partial_{15}$
180	60	-10	-23.5	-4.4	-7.6

**Table 6.** vibrationally resonant nonlinear susceptibilities of CH<sub>3</sub>-Si(111) surface for symmetric and asymmetric C-H stretch modes obtained by fitting the resonant SFG signal for PPP and SSP polarization combinations to equations (14-15)

$\zeta$	$\gamma$	$\partial_{11}^{as}$	$\partial_{33}^{ss}$	$\partial_{31}^{as}$	$\partial_{15}^{ss}$
150	6.7	13	-55	-5	-6.5

## References

- (1) Sipe, J. E.; Moss, D. J.; Vandriel, H. M. *Phys Rev B* **1987**, *35*, 1129.
- (2) Lagutchev, A.; Hambir, S. A.; Dlott, D. D. *J Phys Chem C* **2007**, *111*, 13645.